

Numerical Investigation of the Effects of Impactor Geometry on Impact Behavior of Sandwich Structures

Ilyas BOZKURT^{1*}

¹*Department of Mechanical Engineering, Architecture and Engineering Faculty, Muş Alparslan University, Muş, Türkiye.*
(ORCID: [0000-0001-7850-2308](https://orcid.org/0000-0001-7850-2308))



Keywords: Impactor shape effect, Sandwich composite, Impact test, Progressive damage analysis, Cohesive zone model (CZM), Finite element method.

Abstract

The aim of this study is to examine the impact performance and damage behavior of sandwich composite structures with a core material of aluminum and a facesheet of glass fiber composites using the finite element method. In the study, the effects of impactor shape, impact velocity and number of core layers on peak force, absorbed energy efficiency, maximum displacement and damage deformation were examined. For low velocity impact simulation, *progressive damage analysis* was performed based on the *Hashin damage criterion* using the *MAT 54* material model in the *LS DYNA* finite element program. While providing the connection between the core structure and its surfaces, a *Cohesive Zone Model (CZM)* based on the *bilinear traction-separation law* was created and examined. At the end of the study, it was determined that the shape of the impactor had a significant effect on impact resistance. Energy absorption efficiency may vary as impact energy changes. However, as the impact energy increases, the energy absorption efficiency increases. It was determined that the largest and dominant damage type for all three impactors was matrix damage.

1. Introduction

Composite structures are used effectively in many sectors, especially in the defense industry, due to their high strength/weight ratios [1]. Especially recently, with the technological developments and the development of production machines and production methods, it has started to be used in many areas in our daily lives, from mobile phone cases to car steering wheels. In addition, the use of composite structures, which are widely used in the aviation and space industry, especially in large passenger aircraft, and which carry life and property, is increasing day by day. However, their performance decreases due to the loads they are exposed to in application areas and during service [2]. Especially under impact load, major damage may occur over time due to delamination that occur in the material structure and are sometimes invisible to the eye. To prevent this, the impact performance and damage behavior of these

structures must be known very well. In addition, since the shape or size of the object causing the impact is not known precisely, the reaction of the material and structure against it is unknown [3]. Therefore, when engineers or researchers design a new structure, they need to review all these possibilities and realize the optimum design within these possibilities.

Determining the behavior of composite structures under load is more difficult than metal materials [4]. Because metal structures have linearity, material reactions and behaviors under load can be predicted. However, it was more difficult to determine this behavior in composite structures. Because after impact is applied to composite structures, different types of damage (such as matrix damage, fiber damage, delamination) occur to absorb this energy. These damages gradually occur to absorb the incoming energy, and then the damage to the structure is completed. In addition, the complex micromechanical structure of composite structures

*Corresponding author: ilyasbozkurt02@gmail.com

Received: 11.05.2024, Accepted: 18.09.2024

makes it difficult for researchers to determine this material behavior. Because there may be composites with very different numbers of fiber bundles, very different types of matrix materials and produced at very different temperatures [5]. The mechanical behavior of these structures is different from each other. Therefore, it is essential to further determine the impact performance and damage behavior of these structures and develop them further.

Many studies have been conducted on the impact performance of composite structures [6-12]. However, there are many studies examining the impact behavior of sandwich composite structures, which have a very high impact absorption potential [13-23]. Manes et al. [24-25] examined the impact performances of foam-based sandwich composites with different densities. Albayrak et al. [26-27] investigated the low velocity impact behavior of curved glass sandwich composites with rubber interlayers. They examined impact performances for different orientation angles and curvature shapes. They carried out numerical simulations using the *LS DYNA MAT 162* material model. Bozkurt et al. [15, 28] examined the effects of structural differences of carbon sandwich composites with different core structures on the impact performance. They successfully applied numerical simulations with the *LS DYNA* finite element model. Xue et al. [29] experimentally and numerically examined the impact behavior of specimens produced using honeycomb core carbon/glass fiber hybrid composite facesheets. Yellur et al. [30] experimentally and numerically examined the effects of upper and lower facesheet thicknesses on impact behavior in polypropylene honeycomb sandwich structures. They used the *LS-DYNA* finite element model for numerical analysis. Susainathan et al. [31] numerically investigated the impact behavior of innovative wood-based sandwich structures with plywood cores and coatings made of aluminum or fiber-reinforced polymer (carbon, glass or flax composite coatings). Numerical models were created with *ls dyna*. Shirbhate et al. [32] examined the explosion response of a hexagonal honeycomb sandwich structure with holes along the cell height of the core compared to conventional honeycomb cores. They performed detailed numerical analysis to accurately reproduce the deformation process by finite element analysis using the open *LS-DYNA* software. Yalkın et al. [33] numerically investigated the low-speed impact properties of E-glass fiber/epoxy and PVC foam core sandwich composite configurations. Numerical simulations were carried out using material models of hard impact, foam core and composite material models of *LS-DYNA* software. Damghani et al. [34] simulated the impact behavior of

aluminum foam core sandwich structures with *LS-DYNA* software. They investigated the effects of foam density on impact performance.

In this study, the impact performance and damage behavior of sandwich composite structures, whose core material is aluminum and facesheet material is glass fiber composite, were examined using the finite element method. In the study, unlike the literature, the effects of impactor shape (cylinder, cone and sphere) impact velocity (10 J, 30 J and 60 J), and number of core layers (1 layer, 2 layers and 3 layers) on peak force, absorbed energy efficiency, maximum displacement and damage deformation were investigated. The energy absorption efficiency values obtained at the end of the study were compared with similar studies in the literature.

2. Material and Method

The dimensions details of sandwich composite specimens with aluminum core and glass fiber composite facesheets are given in Figure 1 and the tests to be performed are given in Table 1. Low velocity impact test will be applied to the specimens whose dimensions are given. The dimensions and shapes of the impactors used in the study are given in Figure 2. The upper and lower holders are fixed to ensure the same boundary conditions as the standard experimental testing mechanism. The impactor was limited to displacements in the x and y directions and could only move in the impactors direction (z-axis).

An eight-node solid element (*ELFORM1*) was used in the modeling. There are many element types in the finite element model. Generally, eight-node solid element types are used in the studies. There are many reasons why this is preferred. First of all, as the number of nodes increases, the processing time increases significantly. Especially in studies where the number of elements is high, the processing time becomes very long. Eight-node solid element types can be intervened more effectively in the calibration process. In addition, the damage criteria coefficients that allow this in the *LS DYNA MAT 54* material model make this process easier. This element type is used in most of the *LS DYNA* applications in the literature. 30197 nodes and 26750 solid elements were used. The lower and upper holders were modeled with 7740 nodes and 5500 solid elements. The CONTACT ERODING SURFACE TO SURFACE contact card was used to model the contact force between the sandwich composite and the impactor. The CONTACT AUTOMATIC SURFACE TO SURFACE contact card was used to prevent the specimen between the holders from moving during impact and to keep it fixed by the

holder. The static and dynamic friction coefficients here are entered as 0.2 and 0.3, respectively [28].

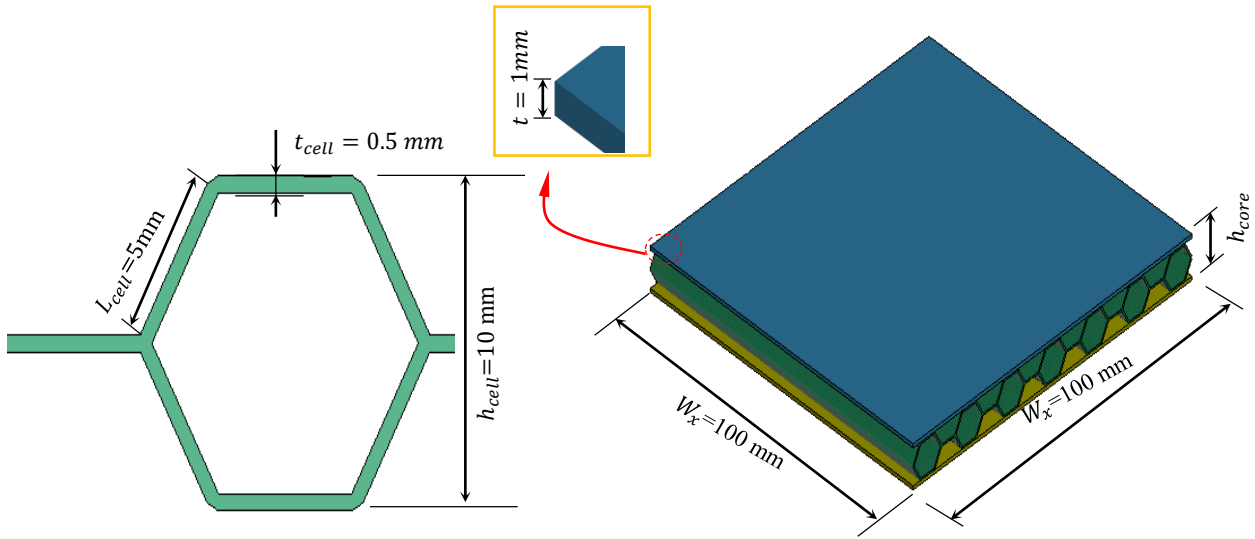


Figure 1. Specimen dimensions.

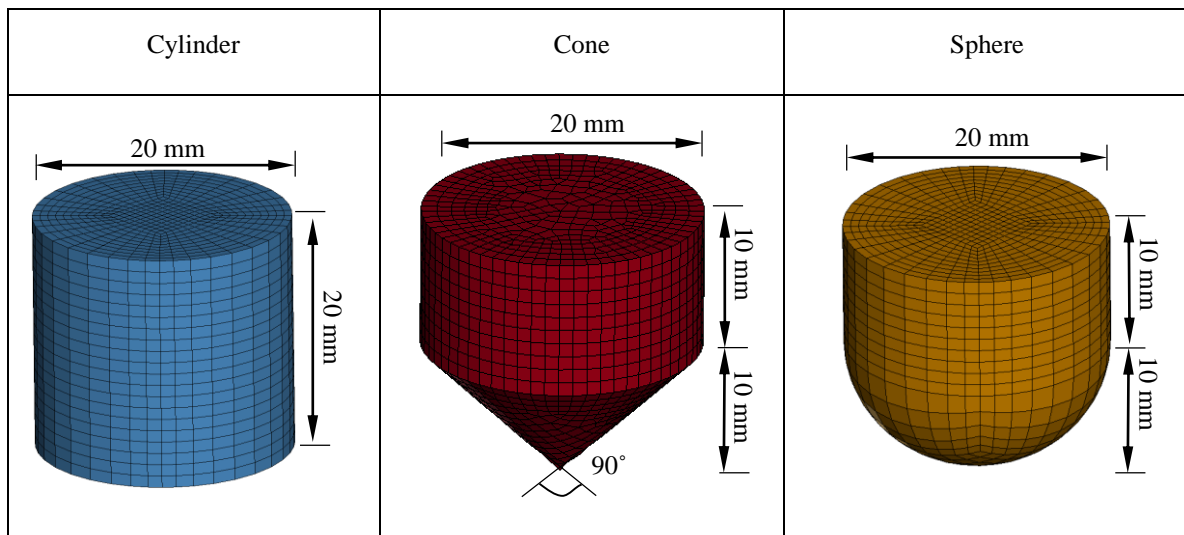


Figure 2. Impactor's dimensions.

The program's solution methodology includes material cards that provide damage models based on the *continuous damage mechanism* (CDM). It allows progressive visualization of structural damage using models based on CDM. Impact tests with dimensions of 100x100 mm were carried out numerically for all specimens used in this research. The mesh size is taken as 2x2 mm. The sandwich composite plate and the upper and lower holders are modeled as shown in Figure 3. As indicated in Figure 4, the impact test was applied to the center of all specimens.

Table 1. Parameters examined for sandwich panels in impact testing.

No	Impactor shape	Core number, n	Impact Energy, E [J]
1	Sphere	1-2-3	10-30-60
2	Cylinder	1-2-3	10-30-60
3	Cone	1-2-3	10-30-60

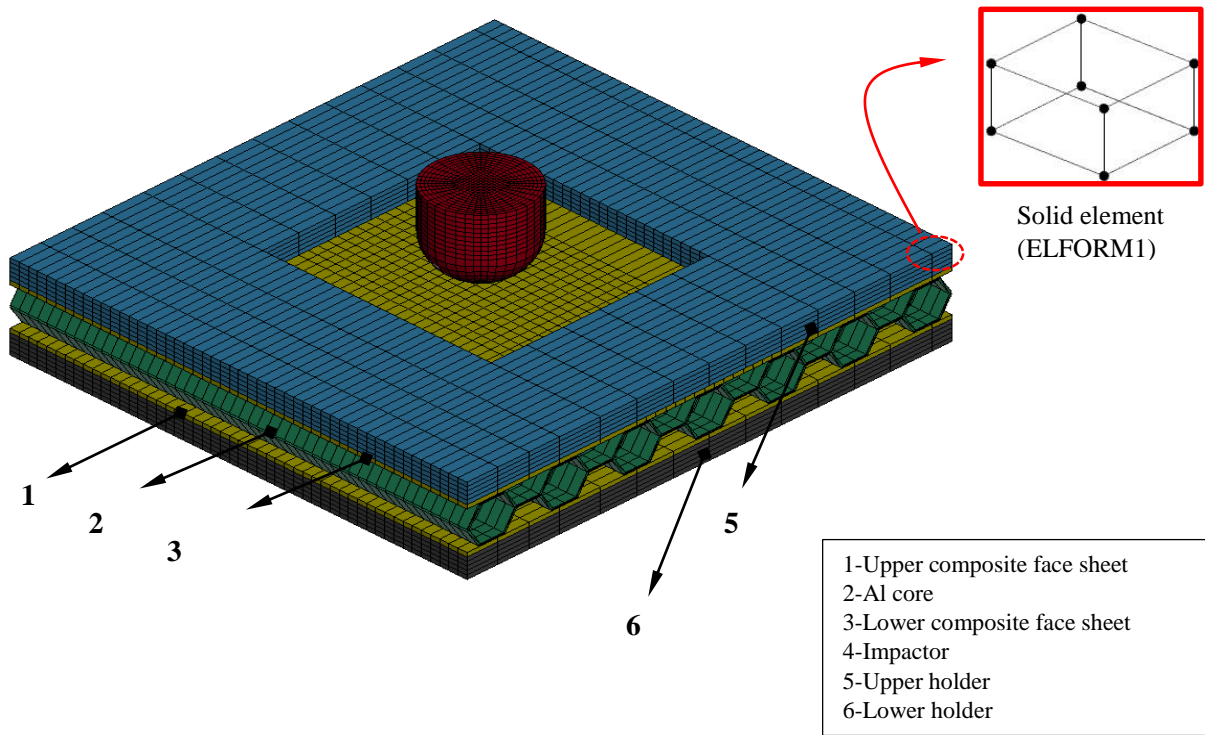


Figure 3. Finite element model of low velocity impact test.

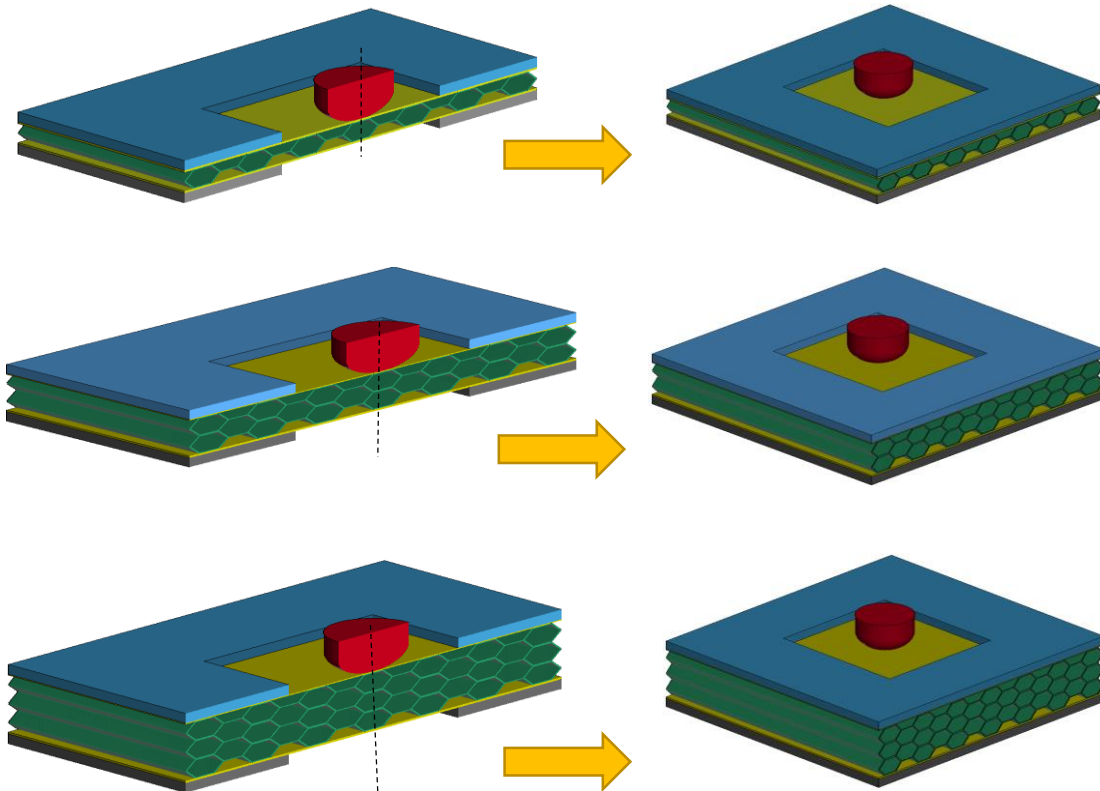


Figure 4. Impact point for sandwich composites with different layer numbers.

Many finite element programs have been developed to determine the impact behavior of aluminum honeycomb glass sandwich specimens. Among these, *LS-DYNA*, a commercial finite element software program, was preferred due to its wide material library, ease of use of interfaces and the ability to develop complex numerical models [35].

In low velocity impact tests, many graphs and data about the mechanical performance of the material are obtained. In these graphics and outputs, it is decided whether the material is suitable for the component or location to be used or not by comparing it with the standards. In the low velocity impact experimental test setup, these data are obtained by reading from the impactor shape. Displacement graphs are derived from the impactor's position along with changes in kinetic energy and velocity. Equations (1)-(4) were used to obtain the changes in velocity, displacement, and energy based on the impactor's impact timing. Data regarding the contact force, displacement and absorbed energy obtained from the impactor were evaluated.

$$v(t) = v_i + gt - \int_0^t \frac{F(t)}{m} dt \tag{1}$$

Here, t is the time of the first contact of the impactor to the specimen, which is $t = 0$; $v(t)$ is the velocity of the impactor at time t ; v_i is the velocity of the impactor at time $t = 0$; and $F(t)$ is the impact contact force measured at time t .

$$\delta(t) = \delta_i + v_i t + \frac{gt^2}{2} - \int_0^t \left(\int_0^t \frac{F(t)}{m} dt \right) dt \tag{2}$$

δ is the displacement of the impactor at time t , while δ_i is the displacement of the impactor from the reference point at time $t = 0$.

$$E_a(t) = \frac{m(v_i^2 - (v(t))^2)}{2} + mh\delta(t) \tag{3}$$

Here, $E_a(t)$ is the absorbed energy at time t , m is the weight impact, and g is the gravitational acceleration. To evaluate the weight efficiency of the energy absorption of a structure, the specific energy absorption (*SEA*) is generally used.

$$SEA = \frac{E_a}{m} \tag{4}$$

Here, m is the mass of the crash structure. Higher *SEA* values indicate better energy-absorbing efficiency of the structures.

2.1. Modeling of Adhesive Layer

Sandwich composite structures are formed by combining the upper and lower facesheets and the core structure between these surfaces. Different applications and methods are used to join these two elements. But this bonding is mostly achieved by using different adhesive types. Determining the mechanical behavior of this structure at the time of impact is very important from an engineering perspective. To model the adhesive behavior between these two elements, a CZM model with a bilinear traction-separation relationship was developed. The basis of this law lies in the application of three independent parameters. The traction between the layers when the force is applied is t_0 , the separation distance that occurs when the damage begins is δ_0 and the remaining under this curve is G_c . After the impact occurs, separation between layers occurs according to this principle (Figure 5)

Adhesion here can be achieved in two ways. This can be achieved by first defining a thin interface material between the top facesheets and the core in the middle. Or, this adhesion can be achieved by using the adhesion surface that performs the same function. Dogan et al. [36] determined that this method is effective instead of using intermediate materials. In this study, The CONTACT_AUTOMATIC SURFACE TO SURFACE TIEBREAK contact card was used to adhere the upper and lower facesheets to the core material in between. While the adhesion here is achieved, as shown in Figure 5, separations occur based on the *bilinear traction-separation law*. With this contact card, the nodes making contact in the beginning connect with each other according to the following criterion.

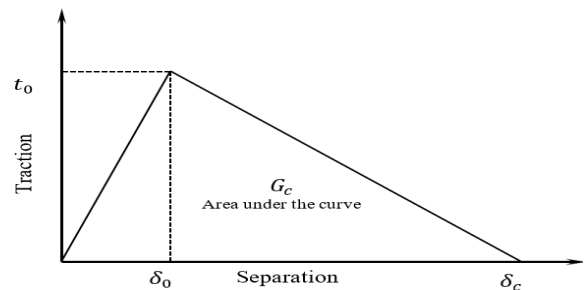


Figure 5. Bilinear traction-separation law.

$$\left(\frac{|\sigma_n|}{NFLS}\right)^2 + \left(\frac{|\sigma_s|}{SFLS}\right)^2 \geq 1 \tag{5}$$

Here, while σ_n and σ_s are the current normal and shear stresses, *NFLS* and *SFLS* are respectively the interface and shear strength. When the condition of Equation (5) is met, interface node stress is decreased to zero and the connection between the nodes is released. The contact parameters for *Araldite 2015*, which was used as the adhesive material in this research, are provided in Table 2.

Table 2. Cohesive parameters of delamination between core and face sheets interfaces [15].

Contact Tiebreak Variable	Value	Units
<i>NFLS</i>	21.63x10 ⁹	Pa
<i>SFLS</i>	17.9x10 ⁹	Pa
<i>PARAM</i>	1	-
<i>ERATEN</i>	430	N/m
<i>ERATES</i>	4700	N/m
<i>CT2CN</i>	1	-
<i>CN</i>	8080	Pa/m

2.3. MAT_54-55: Enhanced Composite Damage Model

The mechanical properties of the GFRP material used in the study are given in Table 3-4 and the mechanical properties of the Al 6061-T6 core material are given in Table 5. The most used model in the analysis of composite structures is the *MAT_54-55* material model. If there is no damage in the material model, the material is assumed to be orthotropic and linear elastic. In this model, *MAT 54* damage criterion was proposed by Chang and *MAT 55* damage criterion was proposed by *Tsai-Wu*. Although the working logic of this material model and the *MAT 22* model is the same, it additionally includes the compression damage mode. The Chang–Chang criterion (*MAT_54*) is given below; Tensile fibre ($\sigma_{11} > 0$).

$$\left(\frac{\sigma_{11}}{S_1}\right)^2 + \bar{\tau} = 1 \tag{6}$$

All moduli and Poisson’s ratios are set to zero when the tensile fibre failure criteria are met, that is $E_1 = E_2 = G_{12} = \nu_{12} = \nu_{21} = 0$ All the stresses in the elements are reduced to zero, and the element layer has failed.

Failure mode for compressive fibre ($\sigma_{11} > 0$),

$$\left(\frac{\sigma_{11}}{S_{12}}\right)^2 = 1 \tag{7}$$

Failure mode for tensile matrix ($\sigma_{11} > 0$),

$$\left(\frac{\sigma_{22}}{S_2}\right)^2 + \bar{\tau} = 1 \tag{8}$$

Failure mode for compressive matrix

$$\left(\frac{\sigma_{22}}{2S_{12}}\right)^2 + \left[\left(\frac{C_2}{2S_{12}}\right) - 1\right] \frac{\sigma_{22}}{C_2} + \bar{\tau} = 1 \tag{9}$$

Where E_1 and E_2 are the longitudinal and transverse elastic moduli, respectively, G_{12} is the shear modulus, ν_{12} and ν_{21} are the in-plane Poisson’s ratios.

Table 3. Mechanical parameters of the GFRP composite [37].

Symbol	Value	Unit
ρ	1500	kg/m ³
E_a, E_b	19	GPa
E_c	6	GPa
ν_{ab}	0.162	-
ν_{bc}	0.162	-
ν_{ca}	0.162	-
G_{ab}	3.786	GPa
G_{bc}	1.709	GPa
G_{ca}	1.709	GPa
S_{aT}	0.459	GPa
S_{aC}	0.2238	GPa
S_{bT}	0.459	GPa
S_{bC}	0.2238	GPa
S_{ab}	0.0828	GPa

Table 4. Failure parameters of the GFRP composite [37].

Symbol	Unit
<i>DFAILM</i>	0.0
<i>DFAILS</i>	0.0
<i>DFAILT</i>	0.0
<i>DFAILC</i>	0.0
<i>TFAIL</i>	0.16
<i>Alpha</i>	0.0
<i>Soft</i>	0.7
<i>FBRT</i>	1
<i>YCFAC</i>	3
<i>EF5</i>	0.90

Table 5. Mechanical properties of Al 6061-T6.

Density (kg/m ³)	E (GPa)	Poisson ratio	Yield stress (MPa)	Failure strain
2850	72	0.33	252	0.4

3. Results and Discussion

Impact simulations were carried out in the *LS DYNA* finite element program to determine the impact behavior of sandwich composite specimens with Aluminum T6061 core and GFRP facesheets. Impact testing results in three different scenarios. The impactor may bounce back from the specimen's surface. It loses some of its energy but then continues with a certain energy. This is called rebounding. The impactor may get stuck in the specimen and its velocity will decrease to zero. Here, the specimen absorbed all the energy of the impactor. This is called penetration. If the impactor pierces the specimens and comes out from the back surface, it is called perforation [15]. The name of an impact test may change depending on the velocity of the impactor. If the impactor's velocity is less than 10 m/s, it is called a low velocity impact. If it is between 10-50 m/s, it is called medium velocity impact, and if the impactor's velocity is more than 50 m/s, it is called high velocity impact [21]. These studies are mostly used for ballistic research. Three different impactor types were used in this study. These are Sphere, Cylinder and Cone. The width and height of these impactors are the same, but their volumes are different. Therefore, in order to perform an impact test with the same energy values, it is necessary to have different velocities. Impact tests were carried out at three different energies: 10 J, 30 J and 60 J. The specimens used in the study include 1-layer core specimen, 2-layers core

specimen and 3-layers core specimen. Separate situations have been evaluated for these.

In Figure 6, variation of contact force-time, energy-time, contact force-displacement and velocity-time graphs with impactor geometry are given for 10 J. When the contact force-time graph is examined in Figure 6a, the contact force for the cylinder impactor reached a maximum point of 11.43 kN and then returned to the zero point. The impactor rebounded from the specimen surface. This impact phenomenon is called rebounding. It has been determined that there are no sharp oscillations on the graph. It was observed that the impact process was completed without damaging the layers. When the graph for the sphere impactor is examined, the contact force reaches a peak of 4.58 kN and a sharp decrease in force occurs. Here it is understood that the upper surface is damaged. In the cone impactor, it has been observed that the force decreases sharply after a shorter period of time compared to other impactor types. The reason for this is that the impactor shape is sharper than the others. When the energy-time graph in Figure 6b is examined, an impact simulation was applied with an impact energy of 10 J for all three impactors. However, the remaining energies at the end of the impact are different from each other. While the initial energy for the sphere impactor is 10 J, the energy after the impact is 1.32 J. When the energy in the final state is subtracted from the energy in the initial state and divided by the initial energy, the absorbed energy efficiency value is obtained. This value was determined as 0.86 for sphere impactor, 0.79 for cylinder impactor and 0.97 for cone impactor. When the contact force-displacement graph is examined in Figure 6c, the maximum displacement occurred as 2.96 mm in case of impact with the cylinder impactor. It is observed for all specimens that after the impactor contacts the specimen, the displacement increases with the force, and then the force and displacement reach zero values. In Figure 6d, it was determined that changes occurred in the velocity-time graph in parallel with the energy-time graph. More detailed results of these graphs will be given in the next section.

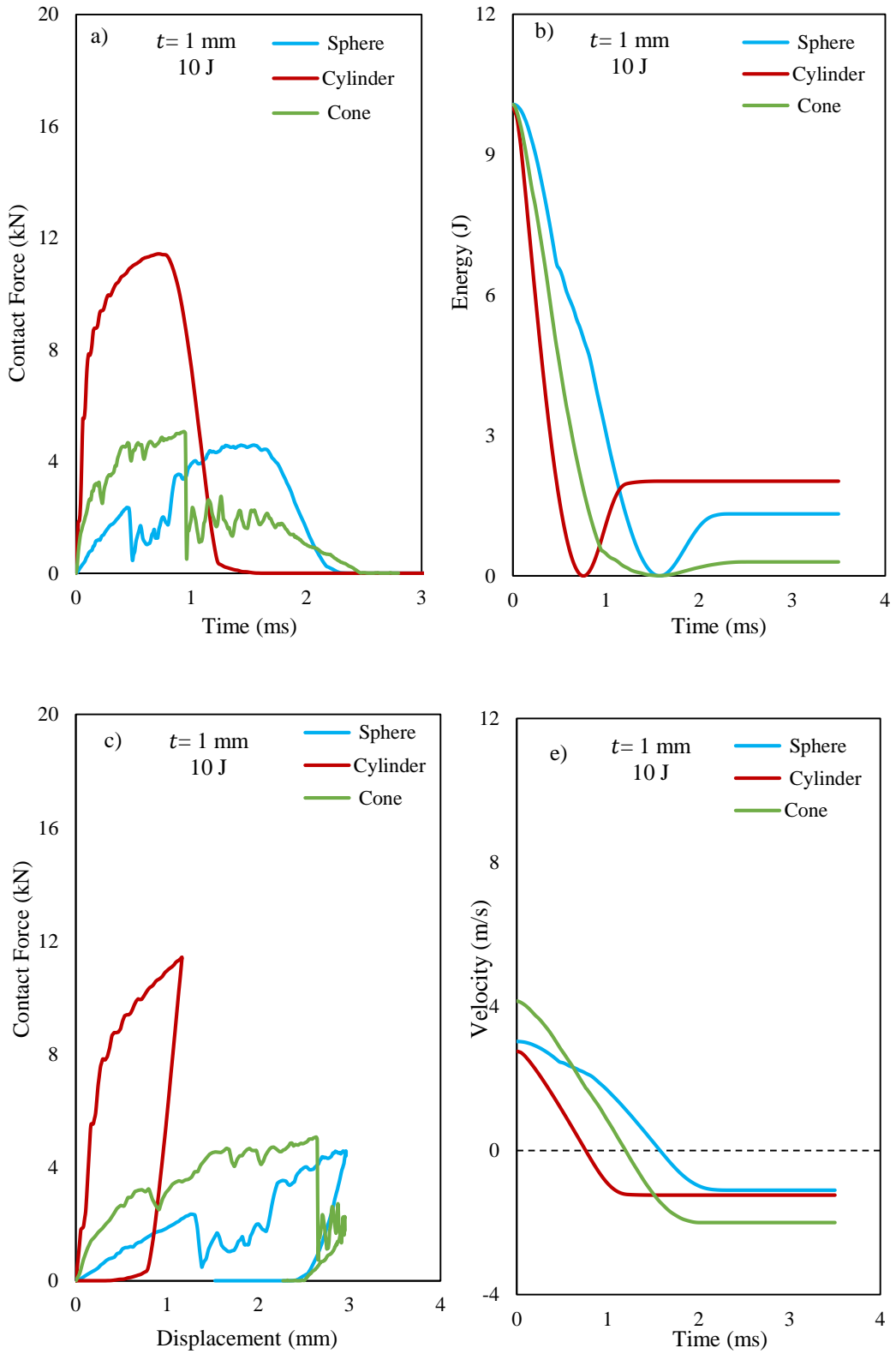


Figure 6. Variation of a) Contact force-Time, b) Energy-Time, c) Contact force-Displacement and d) Velocity-Time graphs with impactor geometry (10 J).

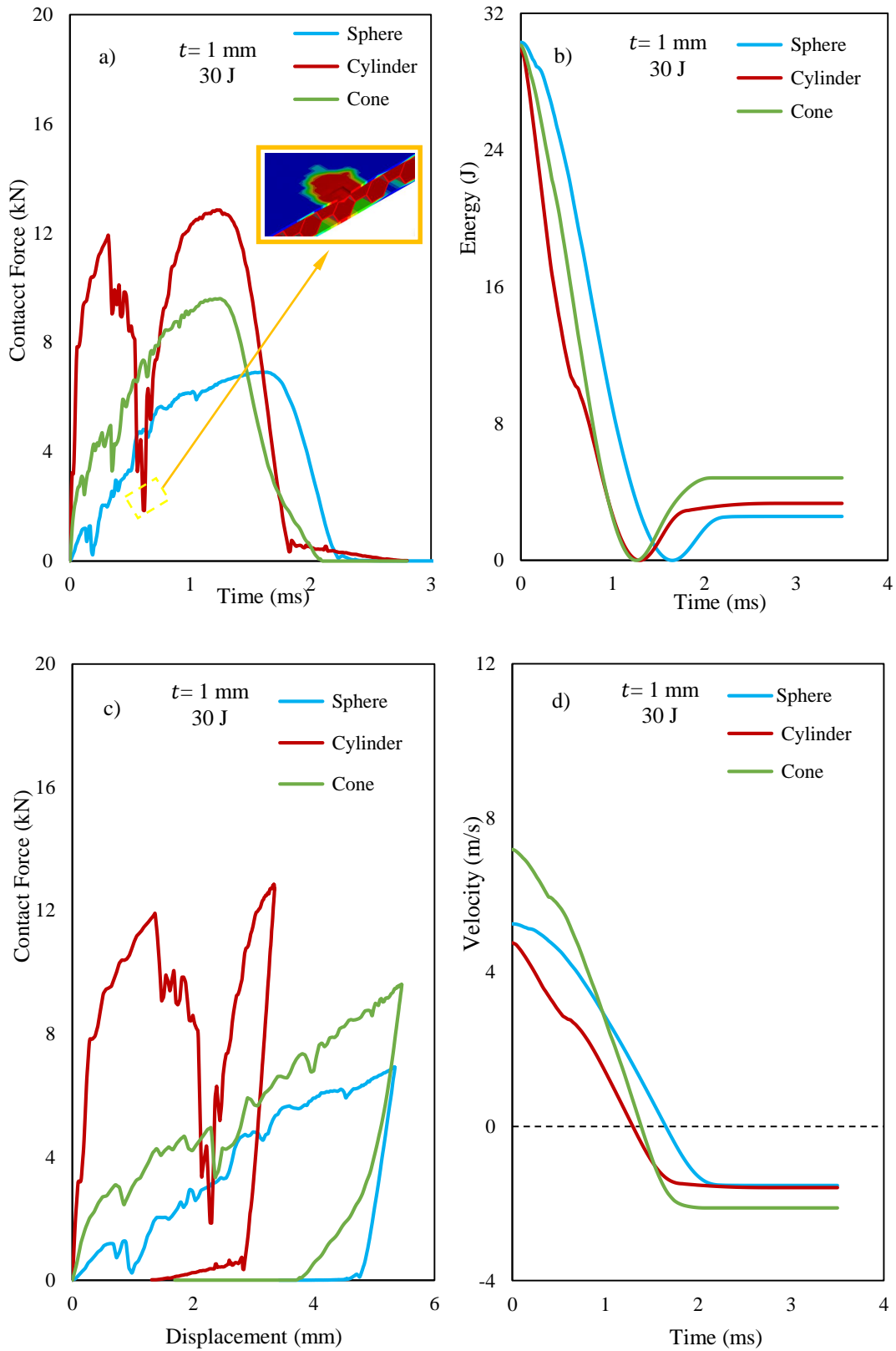


Figure 7. Variation of a) Contact force-Time, b) Energy-Time, c) Contact force-Displacement and d) Velocity-Time graphs with impactor geometry (30 J).

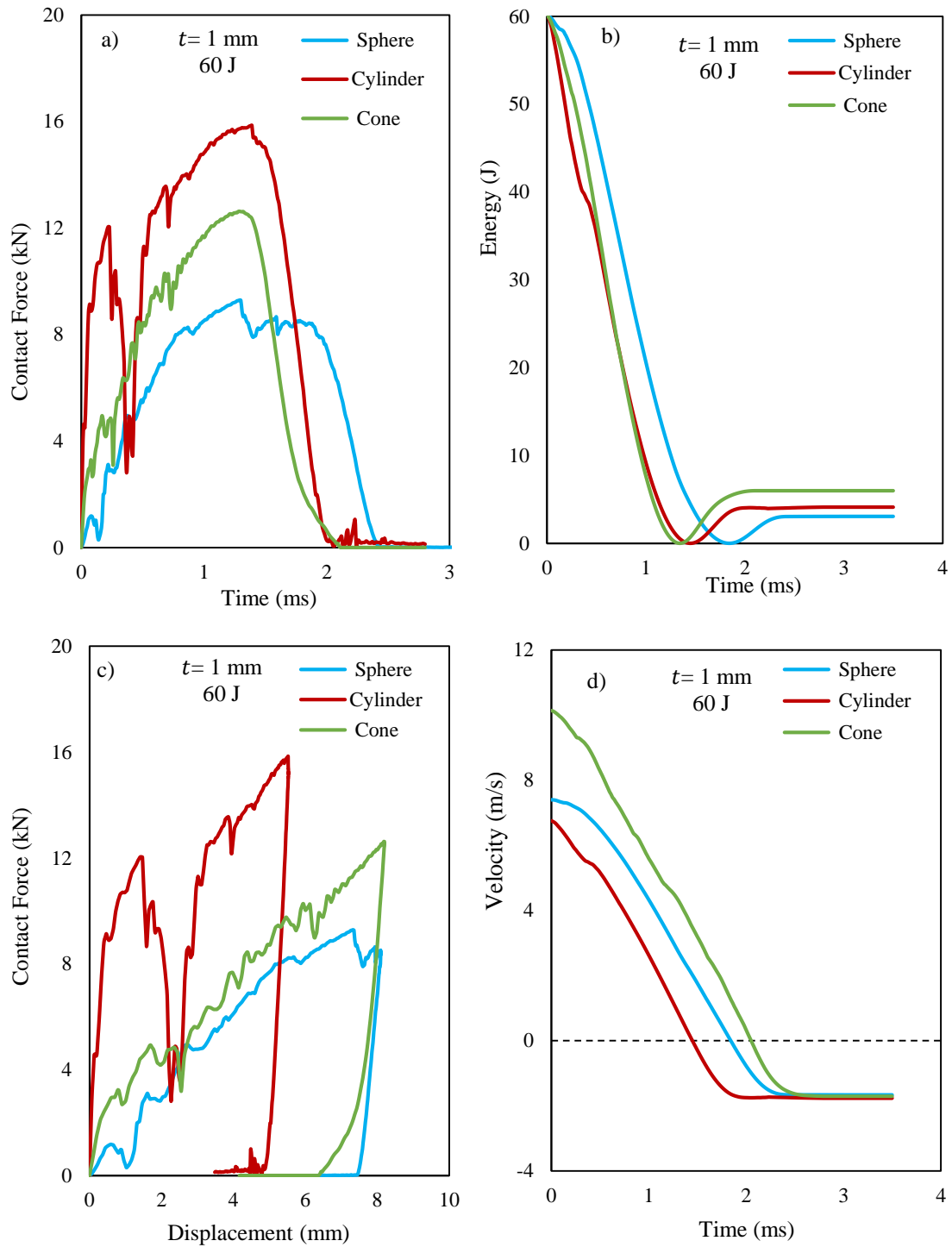


Figure 8. Variation of a) Contact force-Time, b) Energy-Time, c) Contact force-Displacement and d) Velocity-Time graphs with impactor geometry (60 J).

Variation of contact force-time, energy-time, contact force-displacement and velocity-time graphs with impactor geometry are given in Figure 7 for 30 J and in Figure 8 for 60 J. The general evaluation of these graphs will be made through Figure 9. In Figure 9, peak force, energy absorption efficiency and

maximum displacement values of impactor types for 10 J, 30 J and 60 J are compared using 1-layer core specimen. In Figure 9a, peak force values for cylinder, cone and sphere were obtained as 11.42 kN, 5.07 kN and 4.58 kN, respectively, at 10 J impact energy. It was determined that the highest contact

force was obtained with the cylinder impactor if all three specimens were impacted with equal impact energy. The reason for this is that as the contact surface area increases, the time for damage to the material becomes longer. Therefore, the contact time continues to increase until the energy runs out [26]. When looking at the energy absorption efficiency value, it was determined as 0.79, 0.97 and 0.86 for cylinder, cone and sphere, respectively. The maximum displacement values were 2.96 mm in the test performed with the sphere impactor. When the impact energy increased from 10 J to 30 J, it was determined in Figure 9b that the contact force and maximum displacement value increased for all three specimens. Energy absorption efficiency value varies. In other words, while this value decreases for the cone impactor, it increases for the cylinder and sphere impactor. It was determined that when the impact energy was 60 J, the contact force and maximum displacement value increased in parallel. When energy absorption efficiency values are compared between 10 J and 60 J for cylinder, cone and sphere, changes occurred as 16.2%, -7.26% and 9.27%, respectively. In general, as the impact energy increased for the cylinder and sphere impactor, the energy absorption efficiency value of the specimens also increased. In cone impactor, the absorption rate varies because material damage occurs in the specimen structure caused by the impactor. In Figure 10, peak force, energy absorption efficiency and maximum displacement values of impactor types for 10 J, 30 J and 60 J are compared using a 2-layer core specimen. When the number of layers increased from 1 to 2, the peak force value for the cylinder impactor at 10 J decreased by 39%, while the peak force values for the cone and sphere impactor increased by 21.9% and 38.8%, respectively. In Figure 11, peak force, energy absorption efficiency and maximum displacement values of impactor types for 10 J, 30 J and 60 J are compared using a 3-layer core specimen. As the impact energy increases, the peak force value also increases in parallel. The maximum displacement value increases for the same impact energy as the number of layers increases.

In Table 6, the damage deformations occurring on the specimen for cylinder, cone and sphere for 10 J are given. The *LS DYNA MAT-54* material model and the ability to see different damages offered to users were used here [38]. Tensile fiber mode, Compressive fiber mode, Tensile matrix mode and Compressive matrix damage modes occurring in the specimen were shown separately.

The areas shown here in red indicate the damage to the structure. The areas shown in blue represent areas where damage has not occurred yet. The colors between these two color scales can be determined from here whether damage is close at the fringe level. Total stress values are calculated for the initiation of damage in an element. When these stress values reach the yield strength of this element, that is, 1, damage occurs here and the element at this point is deleted in the finite elements [15]. The force then passes to the other element. When the impact results with different impactors are examined in Table 6, it was determined that the biggest damage type for all three impactors was matrix damage. While damage occurred on the specimen surfaces with all three impact impacts, no damage occurred on the back surface of the specimen for the Tensile fiber mode and Compressive fiber mode [15]. The greatest matrix damage on the front surface occurred in the impact simulation made with the cone impactor. Since the shape of the cone impactor is more pointed than the others, it leaves large deformations on the element it contacts. Therefore, even though the area it contacts is small, it can cause great damage because it leaves a devastating effect [3]. However, the damage area it causes on the back surface is less. Table 7 shows the damages for impact energy of 30 J. It is seen that as the impact energy increases, the damage areas also increase. It is seen that destructive damage increases when the impact energy is 60J [39]. Especially in the test performed with the cone impactor, the upper cover and core structure were severely damaged.

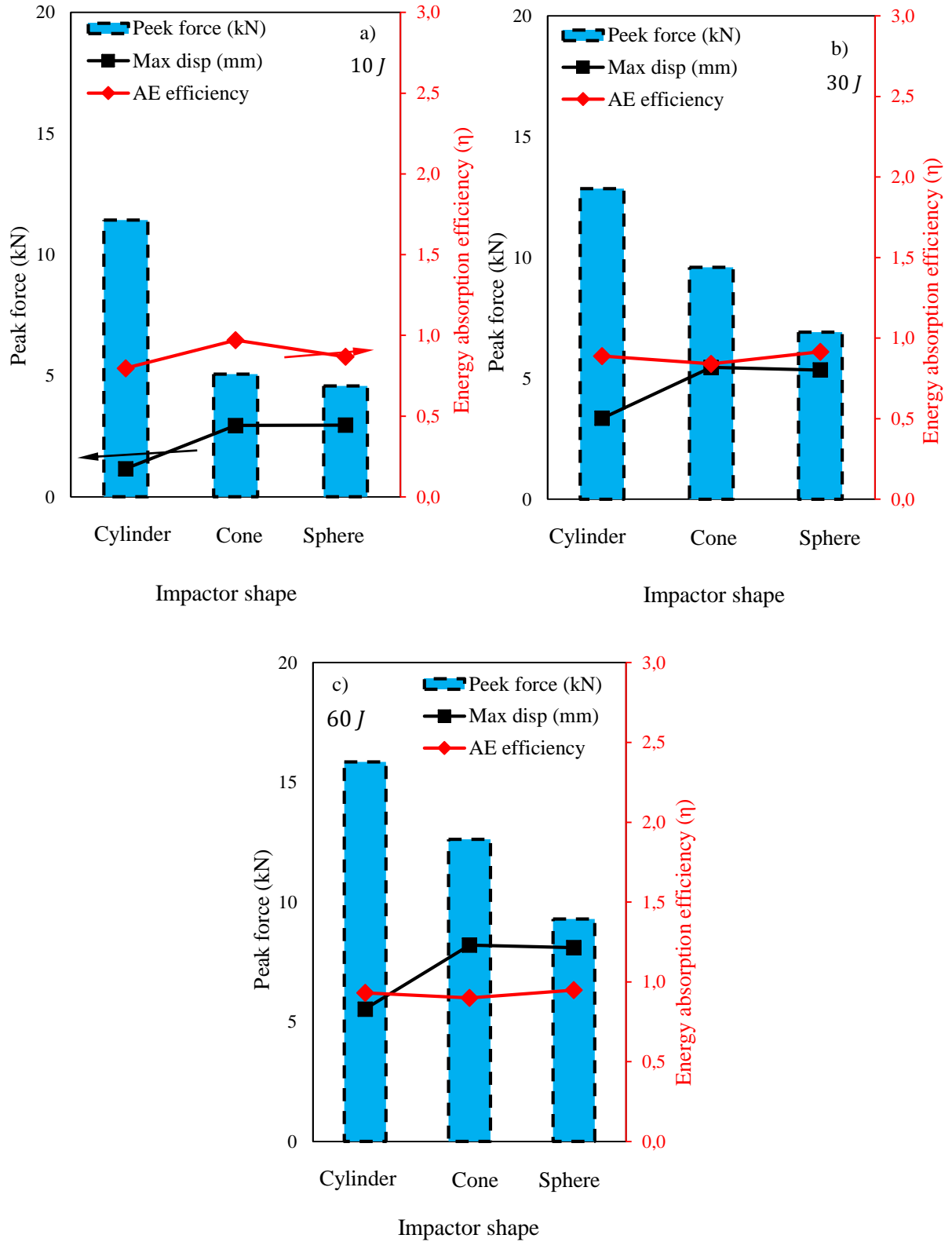


Figure 9. Variation of Contact force, Absorbed energy efficiency, maximum displacement values for a) 10 J, b) 30 J and c) 60 J (1-layer core specimens).

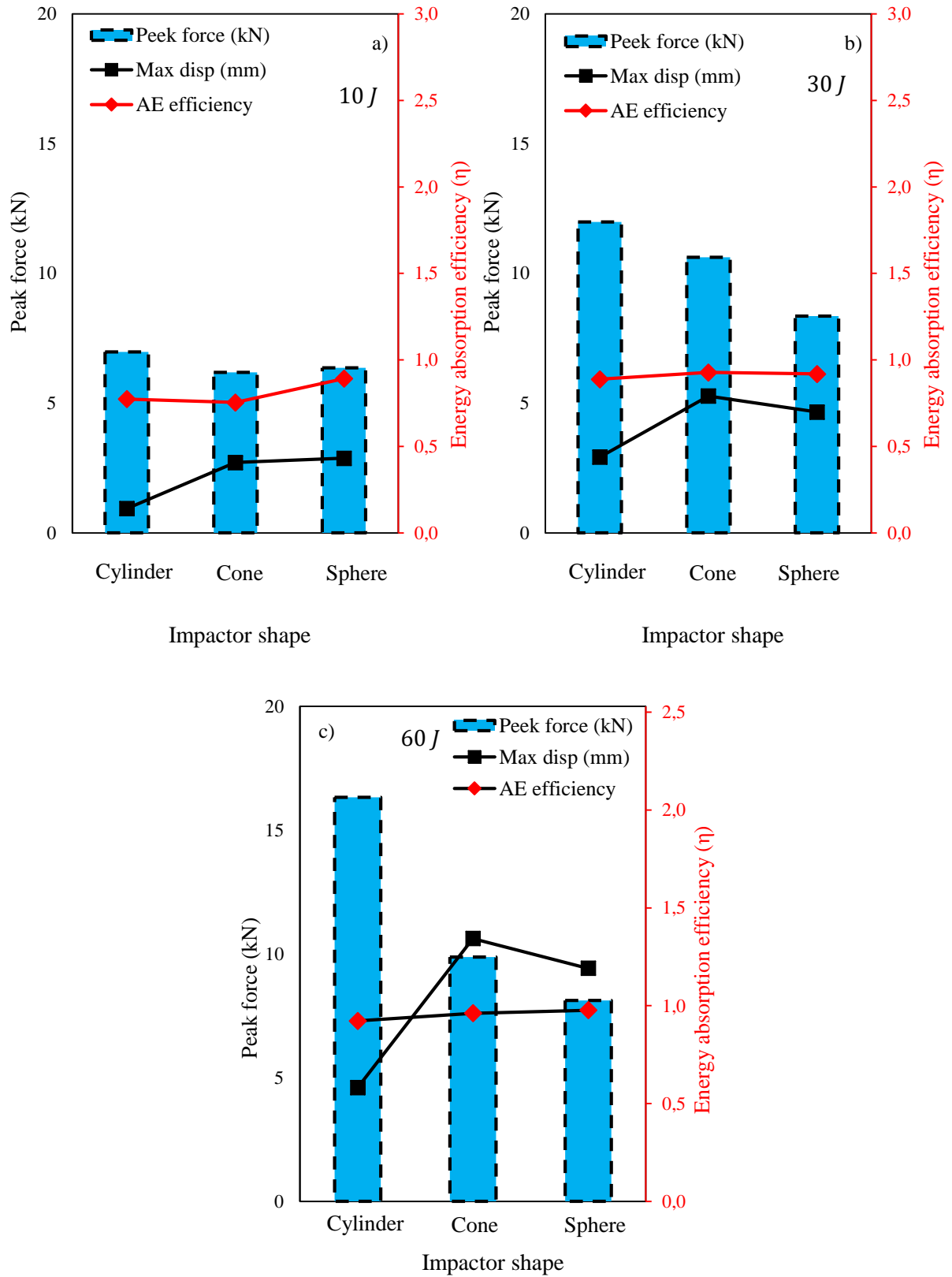


Figure 10. Variation of Contact force, Absorbed energy efficiency, maximum displacement values for a) 10 J, b) 30 J and c) 60 J (2-layer cores specimens).

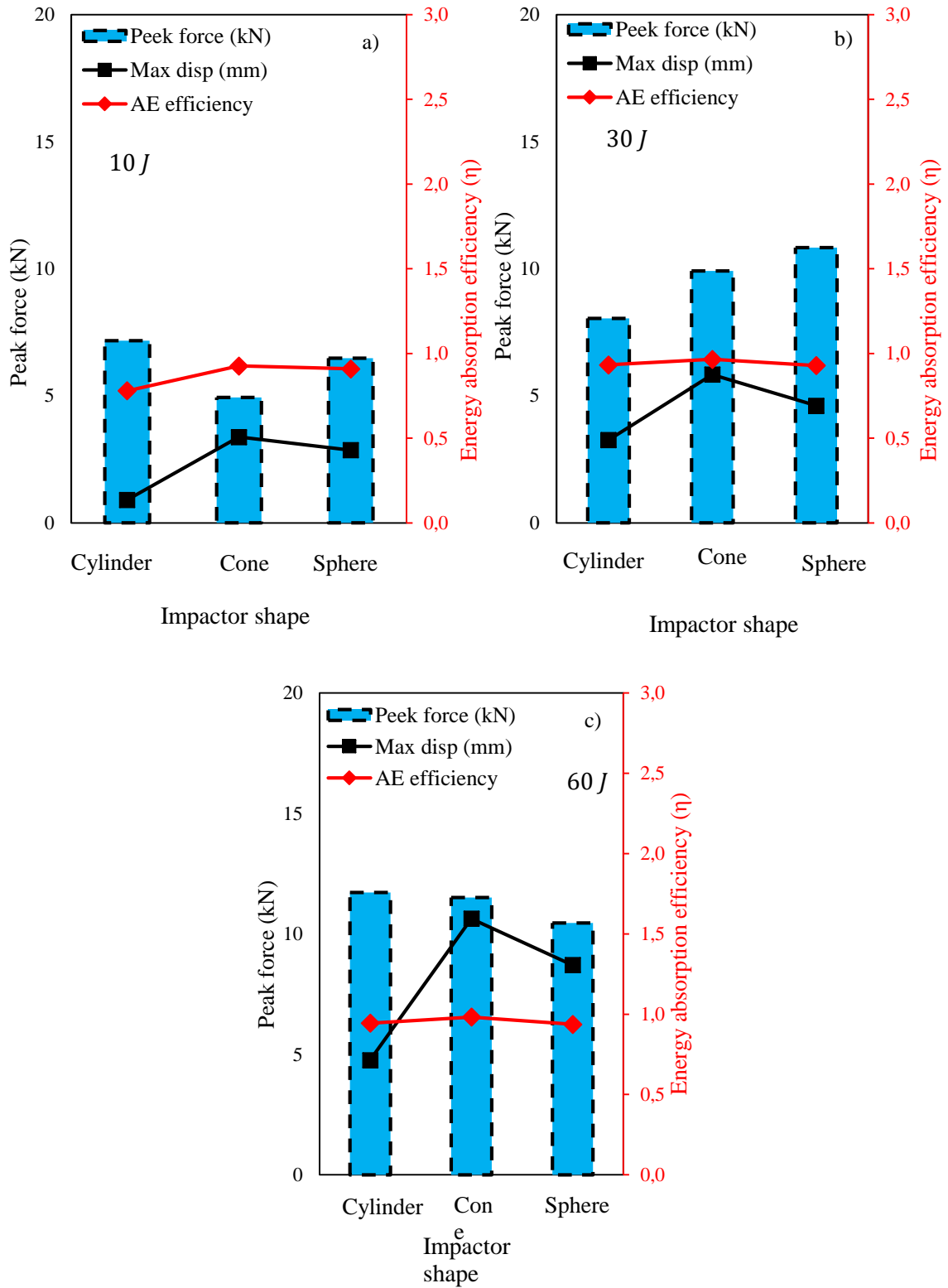


Figure 11. Variation of Contact force, Absorbed energy efficiency, maximum displacement values for a) 10 J, b) 30 J and c) 60 J (3-layer cores specimens).

Table 6. Deformation images under different impactor force [10 J].

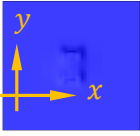
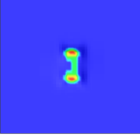
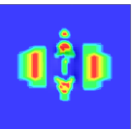
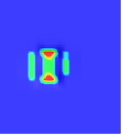


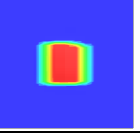

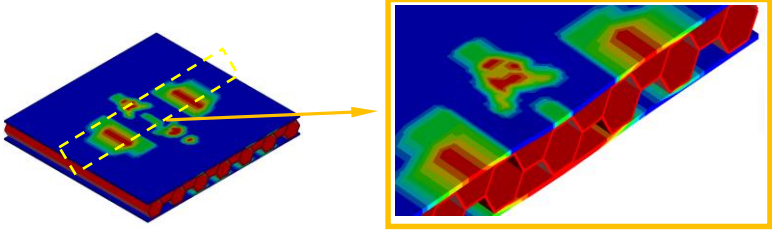
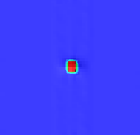
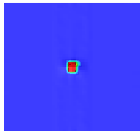
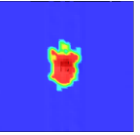
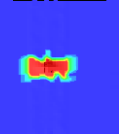
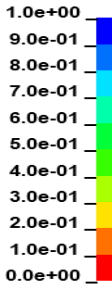
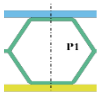


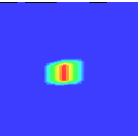

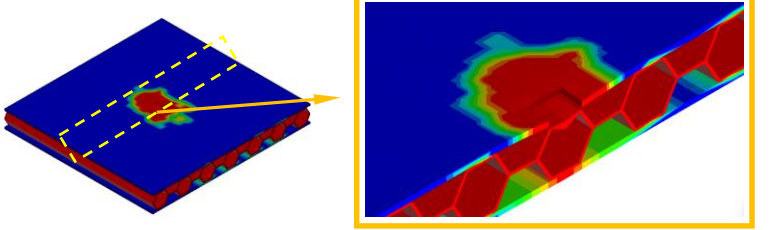
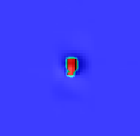
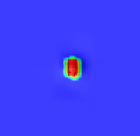
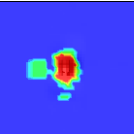
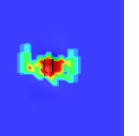


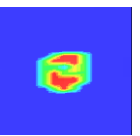

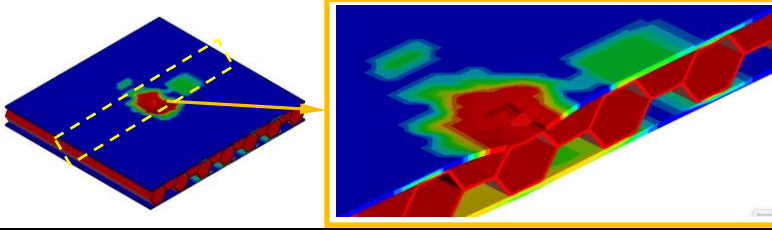
E [J]		Tensile fiber mode	Compressive fiber mode	Tensile matrix mode	Compressive matrix mode	Fringe levels
Cylinder, 10 J	Top face					
	Back face					
	Section view					
Cone 10 J	Top face					 
	Back face					
	Isometric					
Sphere, 10 J	Top face					
	Back face					
	Isometric					

Table 7. Deformation images under different impactor force [30 J].

E [J]		Tensile fiber mode	Compressive fiber mode	Tensile matrix mode	Compressive matrix mode	Fringe levels
Cylinder, 30 J	Top face					
	Back face					
	Section view					
Cone 30 J	Top face					
	Back face					
	Isometric					
Sphere, 30 J	Top face					
	Back face					
	Isometric					

Table 8. Deformation images under different impactor force [60 J].

E [J]		Tensile fiber mode	Compressive fiber mode	Tensile matrix mode	Compressive matrix mode	Fringe levels
Cylinder, 60 J	Top face					
	Back face					
	Section view					
Cone 60 J	Top face					
	Back face					
	Isometric					
Sphere, 60 J	Top face					
	Back face					
	Isometric					

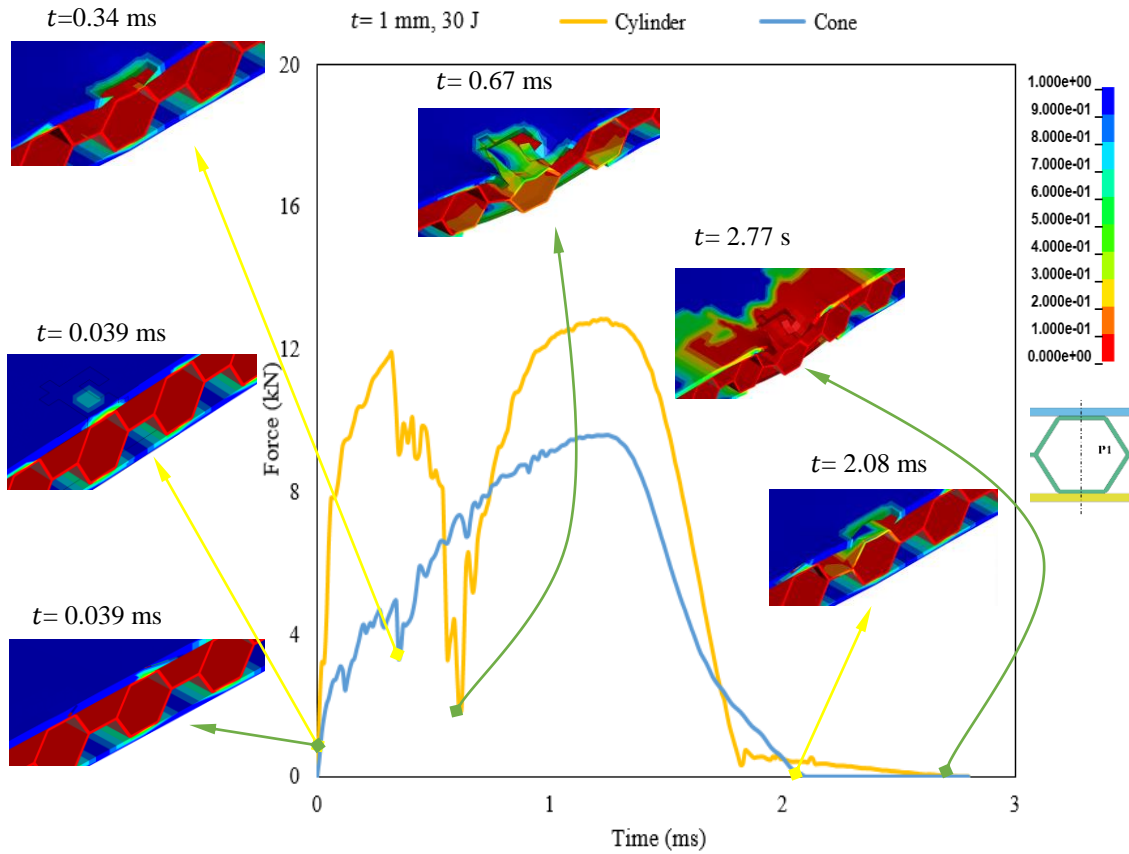


Figure 12. Matrix damage progress graph for cylinder and cone impactor.

When the impactor applies an impact to the specimen surface at a certain velocity, the stress value increases at the point of contact and damage occurs to the elements at this point due to high stresses [26]. This process occurs in a very short time. It is very difficult to follow this damage progression in experimental studies. With developing technology, this damage process can be monitored, at least partially, with high-pixel cameras. Nevertheless, it is difficult to see the damage that occurs in the internal structure of the material during impact. However, the finite element method provides convenience for researchers at this point [5]. The types of damage occurring in the specimen can be seen at any time during the impact. Figure 12 shows the peak force-time graph of impact simulations with cylinder and cone impactors. Here the sphere graph is not included because it is too close to the cone shape and the graph is too complex. When adding matrix damage images, only the images at the critical point were added. Immediately after the impactor contacted the specimen, the stress values in the specimen increased

at $t = 0.039$ ms. It is seen for both specimens that the stress values increase, especially at the point where the impactor contacts and on the back surface just below. In the simulation with the cone impactor, damage occurred on the upper surface at $t=0.039$ ms and the force value decreased accordingly. In the simulation with the cylinder impactor, damage occurred to the upper facesheet at $t = 0.067$ ms, but there was a larger decrease in force. Here, it was determined that damage occurred to the core structure along with the upper cover. In the cone impactor, since the impactor shape is sharp, the facesheet elements at the point of contact are deleted [27]. Therefore, the force decrease occurred to be smaller. At the end of the impact test, in the simulation with the cylinder impactor, the impact test ended at $t = 2.77$ ms and the damage to the facesheet and core structure was caused at the point of contact. In the simulation made with the cone impactor, the impact test ended at $t = 2.08$ ms and damage pictures are shown.

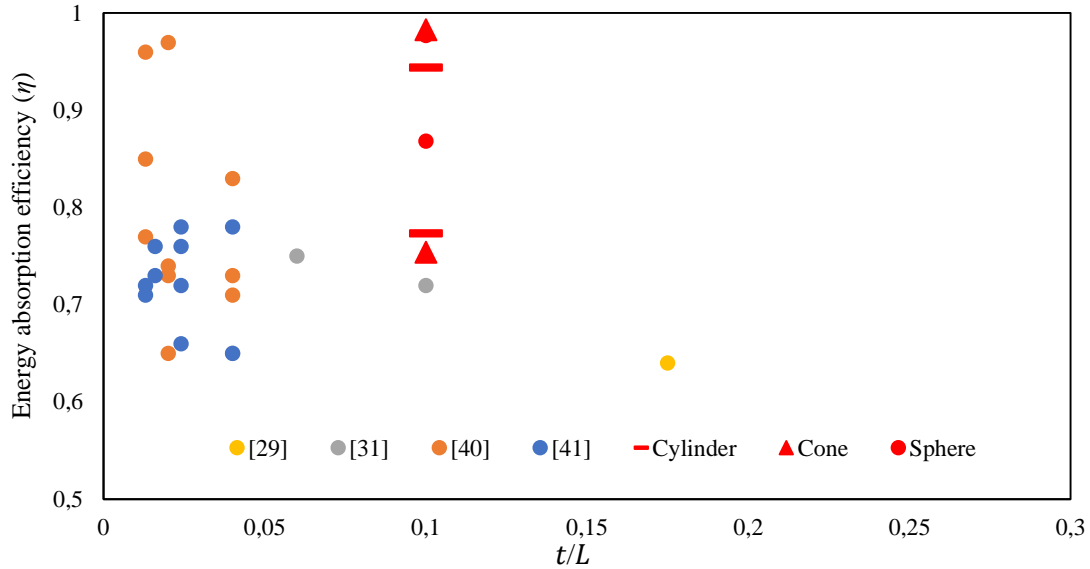


Figure 13. Comparisons of energy absorption efficiencies.

In order to increase the energy absorption efficiency of sandwich composite structures, tests and analyzes have been carried out by making many structural changes. At the end of these tests and analyzes, energy absorption efficiency values are obtained and evaluated to compare their efficiency. The minimum and maximum absorption efficiency values of the sandwich structures used in the current study for different impactors are compared with other studies in the literature [29, 31, 40, 41] with different features and different structures (Figure 13). In the present study, the highest energy efficiency value obtained in the simulation with the cone impactor was found to be 3% higher than the study by He et al [40] and 42.4% higher than the study by Xue et al [29]. What is important here is to determine the optimum dimensions of the sandwich composite structure in terms of engineering by knowing the area of use and the load it will be exposed to. The focus of all these researches is to make the most suitable design for different impactors that the system will be exposed to within the limits of minimum cost and maximum safety.

4. Conclusion and Suggestions

In this study, the impact performance and damage behavior of sandwich composite structures with a core material of aluminum and a facesheet of glass fiber composites were examined using the finite element method. In the study, the effects of impactor shape, impact velocity and number of core layers on

peak force, absorbed energy efficiency, maximum displacement and damage deformation were investigated. For low velocity impact simulation, progressive damage analysis was performed based on the Hashin damage criterion using the *MAT 54* material model in the *LS DYNA* finite element program. The results obtained at the end of the study can be listed as follows;

- The peak force value obtained with the cylinder impactor is higher than other specimens. This is due to the large contact area of the impactor with the specimen.
- In the impact test performed with the cone impactor, the damage time to the specimen is shorter than in the others. Because its impactor shape is sharper, its destructive effect is greater.
- The largest displacement as a result of the impact occurred with the sphere impactor.
- Energy absorption efficiency varies as impact energy changes. But as the impact energy increases, the energy absorption efficiency also increases.
- As the number of layers of the core structure increases, the peak force for the cylinder impactor decreases while the peak force for the sphere and cone impactor increases.
- It was determined that the largest and dominant damage type for all three hitters was matrix damage.

Statement of Research and Publication Ethics

The study is complied with research and publication ethics.

References

- [1] V. Crupi, E. Kara, G. Epasto, E. Guglielmino, and H. Aykul, "Prediction model for the impact response of glass fibre reinforced aluminium foam sandwiches," *Int J Impact Eng*, vol. 77, pp. 97–107, 2015, doi: 10.1016/j.ijimpeng.2014.11.012.
- [2] R. Mohammed, F. Zhang, B. Sun, and B. Gu, "Finite element analyses of low-velocity impact damage of foam sandwiched composites with different ply angles face sheets," *Mater Des*, vol. 47, pp. 189–199, 2013, doi: 10.1016/j.matdes.2012.12.016.
- [3] J. Liu, W. He, D. Xie, and B. Tao, "The effect of impactor shape on the low-velocity impact behavior of hybrid corrugated core sandwich structures," *Compos B Eng*, vol. 111, pp. 315–331, 2017, doi: 10.1016/j.compositesb.2016.11.060.
- [4] İ. Bozkurt, M. Kaman, and M. Albayrak, "LS-DYNA MAT162 Finding Material Inputs and Investigation of Impact Damage in Carbon Composite Plates. XVI. international research conference 2022.," pp. 3–7, 2022.
- [5] M. Albayrak, M. O. Kaman, and I. Bozkurt, "Determination of LS-DYNA MAT162 Material Input Parameters for Low Velocity Impact Analysis of Layered Composites," pp. 39–43, 2022.
- [6] L. Ballère, P. Viot, J. L. Lataillade, L. Guillaumat, and S. Cloutet, "Damage tolerance of impacted curved panels," *Int J Impact Eng*, vol. 36, no. 2, pp. 243–253, Feb. 2009, doi: 10.1016/J.IJIMPENG.2008.03.004.
- [7] R. F. Alshahrani, N. Merah, S. M. A. Khan, and Y. Al-Nassar, "On the impact-induced damage in glass fiber reinforced epoxy pipes," *Int J Impact Eng*, vol. 97, pp. 57–65, Nov. 2016, doi: 10.1016/j.ijimpeng.2016.06.002.
- [8] M. N. Saleh, H. M. El-Dessouky, M. Saeedifar, S. T. De Freitas, R. J. Scaife, and D. Zarouchas, "Compression after multiple low velocity impacts of NCF, 2D and 3D woven composites," *Compos Part A Appl Sci Manuf*, vol. 125, Oct. 2019, doi: 10.1016/j.compositesa.2019.105576.
- [9] J. Krollmann, T. Schreyer, M. Veidt, and K. Drechsler, "Impact and post-impact properties of hybrid-matrix laminates based on carbon fiber-reinforced epoxy and elastomer subjected to low-velocity impacts," *Compos Struct*, vol. 208, no. August 2018, pp. 535–545, 2019, doi: 10.1016/j.compstruct.2018.09.087.
- [10] A. P. Christoforou and A. S. Yigit, "Scaling of low-velocity impact response in composite structures," *Compos Struct*, vol. 91, no. 3, pp. 358–365, Dec. 2009, doi: 10.1016/J.COMPSTRUCT.2009.06.002.
- [11] A. Khodadadi *et al.*, "Numerical and experimental study of impact on hyperelastic rubber panels," *Iranian Polymer Journal (English Edition)*, vol. 28, no. 2, pp. 113–122, Feb. 2019, doi: 10.1007/s13726-018-0682-x.
- [12] Y. Li, F. Wang, X. Shi, L. Guo, and C. Huang, "Impact Response of 3D Orthogonal Woven Composites with Different Fiber Types," *Applied Composite Materials*, 2023, doi: 10.1007/s10443-023-10150-8.
- [13] B. Kazemianfar, M. Esmaeeli, and M. R. Nami, "Response of 3D woven composites under low velocity impact with different impactor geometries," *Aerosp Sci Technol*, vol. 102, Jul. 2020, doi: 10.1016/j.ast.2020.105849.
- [14] M. Y. Solmaz and T. Topkaya, "The flexural fatigue behavior of honeycomb sandwich composites following low velocity impacts," *Applied Sciences (Switzerland)*, vol. 10, no. 20, pp. 1–14, 2020, doi: 10.3390/app10207262.
- [15] I. Bozkurt, M. O. Kaman, and M. Albayrak, "Experimental and numerical impact behavior of fully carbon fiber sandwiches for different core types," *Journal of the Brazilian Society of Mechanical Sciences and Engineering*, vol. 46, no. 5, p. 318, May 2024, doi: 10.1007/s40430-024-04865-3.
- [16] W. He, S. Lu, K. Yi, S. Wang, G. Sun, and Z. Hu, "Residual flexural properties of CFRP sandwich structures with aluminum honeycomb cores after low-velocity impact," *Int J Mech Sci*, vol. 161–162, no. July, p. 105026, 2019, doi: 10.1016/j.ijmecsci.2019.105026.

- [17] W. He, J. Liu, B. Tao, D. Xie, J. Liu, and M. Zhang, "Experimental and numerical research on the low velocity impact behavior of hybrid corrugated core sandwich structures," *Compos Struct*, vol. 158, pp. 30–43, 2016, doi: 10.1016/j.compstruct.2016.09.009.
- [18] Y. Chen, K. Fu, S. Hou, X. Han, and L. Ye, "Multi-objective optimization for designing a composite sandwich structure under normal and 45° impact loadings," *Compos B Eng*, vol. 142, no. December 2016, pp. 159–170, 2018, doi: 10.1016/j.compositesb.2018.01.020.
- [19] X. Zhang, F. Xu, Y. Zang, and W. Feng, "Experimental and numerical investigation on damage behavior of honeycomb sandwich panel subjected to low-velocity impact," *Compos Struct*, vol. 236, no. January, p. 111882, 2020, doi: 10.1016/j.compstruct.2020.111882.
- [20] W. He, J. Liu, S. Wang, and D. Xie, "Low-velocity impact behavior of X-Frame core sandwich structures – Experimental and numerical investigation," *Thin-Walled Structures*, vol. 131, no. July, pp. 718–735, 2018, doi: 10.1016/j.tws.2018.07.042.
- [21] T. K. Demircioğlu, F. Balıkoğlu, O. İnal, N. Arslan, Ay, and A. Ataş, "Experimental investigation on low-velocity impact response of wood skinned sandwich composites with different core configurations," *Mater Today Commun*, vol. 17, no. May, pp. 31–39, 2018, doi: 10.1016/j.mtcomm.2018.08.003.
- [22] J. Wang, A. M. Waas, and H. Wang, "Experimental and numerical study on the low-velocity impact behavior of foam-core sandwich panels," *Compos Struct*, vol. 96, pp. 298–311, 2013, doi: 10.1016/j.compstruct.2012.09.002.
- [23] Y. Rong, J. Liu, W. Luo, and W. He, "Effects of geometric configurations of corrugated cores on the local impact and planar compression of sandwich panels," *Compos B Eng*, vol. 152, no. August, pp. 324–335, 2018, doi: 10.1016/j.compositesb.2018.08.130.
- [24] J. Zhou, M. Z. Hassan, Z. Guan, and W. J. Cantwell, "The low velocity impact response of foam-based sandwich panels," *Compos Sci Technol*, vol. 72, no. 14, pp. 1781–1790, 2012, doi: 10.1016/j.compscitech.2012.07.006.
- [25] A. Manes, A. Gilioli, C. Sbarufatti, and M. Giglio, "Experimental and numerical investigations of low velocity impact on sandwich panels," *Compos Struct*, vol. 99, pp. 8–18, 2013, doi: 10.1016/j.compstruct.2012.11.031.
- [26] M. Albayrak, M. O. Kaman, and I. Bozkurt, "Experimental and Numerical Investigation of the Geometrical Effect on Low Velocity Impact Behavior for Curved Composites with a Rubber Interlayer," *Applied Composite Materials*, vol. 30, no. 2, pp. 507–538, 2023, doi: 10.1007/s10443-022-10094-5.
- [27] M. Albayrak, M. O. Kaman, and I. Bozkurt, "The effect of lamina configuration on low-velocity impact behaviour for glass fiber/rubber curved composites," *J Compos Mater*, vol. 57, no. 11, pp. 1875–1908, 2023, doi: 10.1177/00219983231164950.
- [28] I. Bozkurt, M. O. Kaman, and M. Albayrak, "Low-velocity impact behaviours of sandwiches manufactured from fully carbon fiber composite for different cell types and compression behaviours for different core types," *Materialpruefung/Materials Testing*, vol. 65, no. 9, pp. 1349–1372, 2023, doi: 10.1515/mt-2023-0024.
- [29] X. Xue, C. Zhang, W. Chen, M. Wu, and J. Zhao, "Study on the impact resistance of honeycomb sandwich structures under low-velocity/heavy mass," *Compos Struct*, vol. 226, no. May, p. 111223, 2019, doi: 10.1016/j.compstruct.2019.111223.
- [30] M. R. Yellur, H. Seidlitz, F. Kuke, K. Wartig, and N. Tsombanis, "A low velocity impact study on press formed thermoplastic honeycomb sandwich panels," *Compos Struct*, vol. 225, no. November 2018, p. 111061, 2019, doi: 10.1016/j.compstruct.2019.111061.
- [31] J. Susainathan, F. Eyma, E. DE Luycker, A. Cantarel, and B. Castanie, "Numerical modeling of impact on wood-based sandwich structures," *Mechanics of Advanced Materials and Structures*, vol. 27, no. 18, pp. 1583–1598, Sep. 2020, doi: 10.1080/15376494.2018.1519619.
- [32] P. A. Shirbhate and M. D. Goel, "Investigation of effect of perforations in honeycomb sandwich structure for enhanced blast load mitigation," *Mechanics of Advanced Materials and Structures*, vol. 30, no. 17, pp. 3463–3478, 2023, doi: 10.1080/15376494.2022.2076958.
- [33] H. E. Yalkın, R. Karakuzu, and T. Alpyıldız, "Low-velocity impact behaviors of sandwich composites with different structural configurations of foam core: numerical study and experimental validation," *Phys Scr*, vol. 98, no. 11, Nov. 2023, doi: 10.1088/1402-4896/ad008f.

- [34] M. Nouri Damghani and A. Mohammadzadeh Gonabadi, "Numerical study of energy absorption in aluminum foam sandwich panel structures using drop hammer test," *Journal of Sandwich Structures and Materials*, vol. 21, no. 1, pp. 3–18, Jan. 2019, doi: 10.1177/1099636216685315.
- [35] H. JO., *LS-DYNA Keyword User's Manual Volume II Material Models, Version 971. Livermore Software Technology Corporation; . [24].* 2017.
- [36] F. Dogan, H. Hadavinia, T. Donchev, and P. S. Bhonge, "Delamination of impacted composite structures by cohesive zone interface elements and tiebreak contact," *Central European Journal of Engineering*, vol. 2, no. 4, pp. 612–626, 2012, doi: 10.2478/S13531-012-0018-0.
- [37] M. Albayrak and M. O. Kaman, "Production of Curved Surface Composites Reinforced With Rubber Layer," *European Journal of Technic*, vol. 11, no. 1, pp. 19–22, 2021, doi: 10.36222/ejt.824761.
- [38] A. M. Bozkurt İ, Kaman MO, "LS-DYNA MAT162 Finding Material Inputs and Investigation of Impact Damage in Carbon Composite Plates. XVI. international research conference 2022.," 2022.
- [39] K. Malekzadeh Fard, S. M. R. Khalili, S. H. Forooghi, and M. Hosseini, "Low velocity transverse impact response of a composite sandwich plate subjected to a rigid blunted cylindrical impactor," *Compos B Eng*, vol. 63, pp. 111–122, 2014, doi: 10.1016/j.compositesb.2014.03.011.
- [40] W. He, L. Yao, X. Meng, G. Sun, D. Xie, and J. Liu, "Effect of structural parameters on low-velocity impact behavior of aluminum honeycomb sandwich structures with CFRP face sheets," *Thin-Walled Structures*, vol. 137, no. August 2018, pp. 411–432, 2019, doi: 10.1016/j.tws.2019.01.022.
- [41] Y. Duan, Z. Cui, X. Xie, Y. Tie, T. Zou, and T. Wang, "Mechanical characteristics of composite honeycomb sandwich structures under oblique impact," *Theoretical and Applied Mechanics Letters*, vol. 12, no. 5, p. 100379, Sep. 2022, doi: 10.1016/J.TAML.2022.100379.